Eur Biophys J (2008) 38:53–58
DOI 10.1007/s00249-008-0355-3

ORIGINAL PAPER

Transmission photoemission electron microscopy for lateral mapping of the X-ray absorption structure of a metalloprotein in a liquid cell

D. Panzer · C. Beck · J. Maul · M. Möller · H. Decker · G. Schönhense

Received: 20 November 2007 / Revised: 17 June 2008 / Accepted: 17 June 2008 / Published online: 9 July 2008

Abstract We use photoemission electron microscopy in an X-ray transmission mode for full-field imaging of the X-ray absorption structure of copper in the respiratory metalloprotein hemocyanin KLH1. It contains 160 oxygen binding sites. Each site reversibly binds one molecule oxygen between two copper atoms. In our setup, hemocyanin is dissolved in aqueous solution and enclosed in an ultra-high vacuum compatible liquid sample cell with silicon nitride membranes. The local X-ray absorption structure of the liquid sample is converted into photoelectrons at the microscope side of the cell acting as a photocathode. In this way, different copper valencies are laterally distinguished under in vivo-like conditions, attributed to Cu(I) in the deoxy-state and Cu(II) in the oxy-state.

Keywords X-ray absorption spectroscopy · XANES · X-ray spectroscopy in biophysics · Photoemission · Photoemission electron microscopy (PEEM)

Introduction

Synchrotron-based spectromicroscopy is a powerful tool to obtain both structural and electronic information from mesoscopic systems, rapidly developing with the continuous increase in the availability of tunable high brilliance radiation from third generation light sources and improvements in instrumentation. It can achieve spatial resolution down to 15 nanometers in the case of X-ray microscopy (Chao et al. 2005) and down to ∼3 nanometers with the SMART at BESSY II (i.e., an aberration corrected "spectromicroscope for all relevant techniques"; e.g., Schmidt et al. 2002), allowing for the extraction of intrinsic properties through the X-ray absorption near edge structure (XANES; Stöhr 1992) as the chemical contrast mechanism.

Two basically different microscopic accesses are commonly distinguished: the "photon-in photon-out" techniques, such as transmission X-ray microscopy (scanning TXM; Hitchcock et al. 2005) or X-ray fluorescence microscopy (XRFM; Takeuchi et al. 2000), and the "photon-in electron-out" techniques. The latter include scanning photoemission microscopy (SPEM; Ade 1998), based on focusing X-rays to a small spot using mirror technologies or Fresnel zone plates, and full-field imaging X-ray photoemission electron microscopy (X-PEEM; Bauer 2001) with its particular potential in exploiting X-ray magnetic circular dichroism (Schneider and Schönhense 2002).

X-PEEM requires illumination of the sample from atop, its surface sensitivity being strongly restricted to a few nanometers only by the escape depth of the photoelectrons (Seah and Dench 1979). For photoemission spectromicroscopy of biological samples, that is, which need to be analyzed under in vivo aqueous conditions, the specimen therefore must be penetrated by the X-ray beam thus calling for a transmission experiment. The first approach was presented by Watts et al. (1997).

Here, we demonstrate transmission X-ray photoemission electron microscopy (T-PEEM, Pohl et al. 2004) for the laterally resolved chemical analysis of a liquid biological sample. In our study, we investigate the respiratory copper protein hemocyanin (Hc) found in the hemolymph of multiple arthropods and molluscs (Van Holde et al. 2001; Decker

D. Panzer · J. Maul (✉) · G. Schönhense
Institut für Physik, Johannes Gutenberg-Universität,
Staudinger Weg 7, 55099 Mainz, Germany
e-mail: jmaul@uni-mainz.de

D. Panzer · C. Beck · M. Möller · H. Decker
Institut für Molekulare Biophysik,
Johannes Gutenberg-Universität,
Welderweg 26, 55099 Mainz, Germany

2005). Its biological function is related to the reversible binding of molecular oxygen to a dinuclear copper active site (Solomon et al. 1992). In early XAS studies, various details of the active-site geometry were determined (e.g., a Cu–Cu distance of ~3.5 Å in oxy Hc; Sabatucci et al. 2002), but overall the picture still remains fuzzy, for example, with respect to the O_2 binding mode. To perform XANES spectromicroscopy, X-ray photon energies are scanned across the L-edge of copper. Thereby, the XANES fingerprint is closely connected to the different copper binding states.

Of course, T-PEEM for spectromicroscopy in aqueous environment is not restricted to hemocyanin, but can also be applied to other metalloproteins including practically all biologically relevant transition metals.

The transmission photoemission electron microscope

The basis of the transmission photoemission electron microscope is a conventional PEEM ("IS-PEEM", Focus GmbH) with two essential modifications: The piezo-driven integrated sample stage (IS) is modified for photon beam transmission from the reverse side of the sample, and a novel delayline detector ("DLD-3636", Surface Concept GmbH; Oelsner et al. 2001, 2004) is used for lateral photoelectron detection.

Figure 1a illustrates the schematic setup of the T-PEEM, consisting of a transmission sample stage, electrostatic lenses (objective lens and two projective lenses), contrast apertures between 1,500 and 30 µm, electrostatic deflectors and stigmators, and the delayline detector (DLD) for data acquisition. The field of view can be varied between ~1 mm in the survey mode and down to <10 µm in the high resolution mode.

The DLD includes a Chevron-type microchannel plate (MCP) configuration for high secondary electron gain and two sequentially arranged flat solenoids (Fig. 1b), here drawn as meanders. In brief, the delayline detector measures the coincidence of electronic impulses that each secondary electron avalanche induces in the pair of perpendicularly oriented flat solenoids. Electron localization and subsequent image processing is realized from the electronic runtime differences recorded at the ends of the solenoids. Since only electronic coincidences are recorded with the DLD, signal-to-noise is strongly enhanced in comparison to conventional imaging tools, such as a MCP combined with a phosphor screen.

Figure 1c, d shows the transmission sample stage with parts of the objective lens of the PEEM from two different views. Precise remote adjustment of the sample position is facilitated by a crossed pair of linear piezo motors. The liquid sample cell is exchangeable in the UHV by means of a load lock system (see arrow).

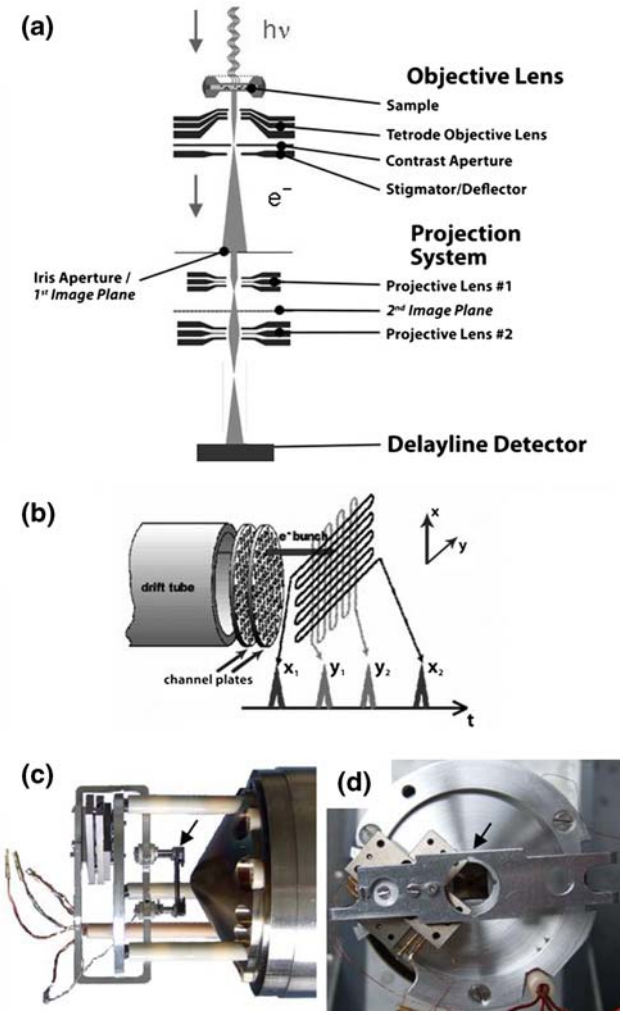

Fig. 1 Different views and illustrations of the T-PEEM setup. **a** Electron optical system of the PEEM combined with the transmission sample stage; **b** detection scheme of the delay line detector (DLD); **c** and **d** transmission sample stage with parts of the PEEM objective lens (*arrows* indicate sample insertion and hole for X-ray transmission, respectively)

The liquid sample cell

The liquid sample cell is composed of two silicon nitride membranes (SPI Supplies), each with a 100 nm thick Si_3N_4 window for transillumination. The sample droplet is transferred to one membrane which is subsequently encircled by an UHV compatible glue (3 M Scotch-Weld, Epoxy adhesive DP-460), the membrane counterpart then being mounted from atop so that the windows face each other. The glue itself becomes unsolvable directly after contact with the water front (as we verified in the laboratory) and should not notably interact with the liquid sample afterwards. In addition, a TEM grid is attached to the back side of the cell to produce a shadowgraph from the photon beam

passing through thus defining a coordinate system for laterally resolved sample analysis.

Figure 2 illustrates the liquid cell construction and the experiment implementation. At photon energies above the Si_3N_4 work function threshold (~ 4.7 eV), in particular for X-rays, the absorption pattern of the photon beam is converted into a lateral photoelectron distribution which is recorded by the PEEM. Thereby, the recorded absorption pattern is a superposition of the TEM grid absorption, the membrane absorption and the sample absorption.

In Figure 3a, a PEEM sample mount with Si_3N_4 membrane in the centre part is shown. The 100 nm membrane with the TEM grid behind is more clearly seen in the enlarged view of Fig. 3b. For laboratory test of the T-PEEM setup, a double membrane cell filled with water was illuminated from the back side at near normal incidence using a broadband high pressure mercury lamp with dielectric mirror for suppression of thermal radiation (FOCUS GmbH, photon energies up to 5.2 eV). The TEM grid structure with a mesh width of 85 µm is clearly recognized in the low magnification mode of the microscope (Fig. 3c). The thickness d of the solution layer enclosed can be roughly estimated by the deposited drop volume of $\leq$0.1 µl and by the area encircled by the glue (~12 mm^2), resulting in $d \leq 8$ µm.

In contrast to conventional PEEM, charging due to topography or insulating samples does not occur in T-PEEM, given sufficiently conducting and sufficiently flat membranes.

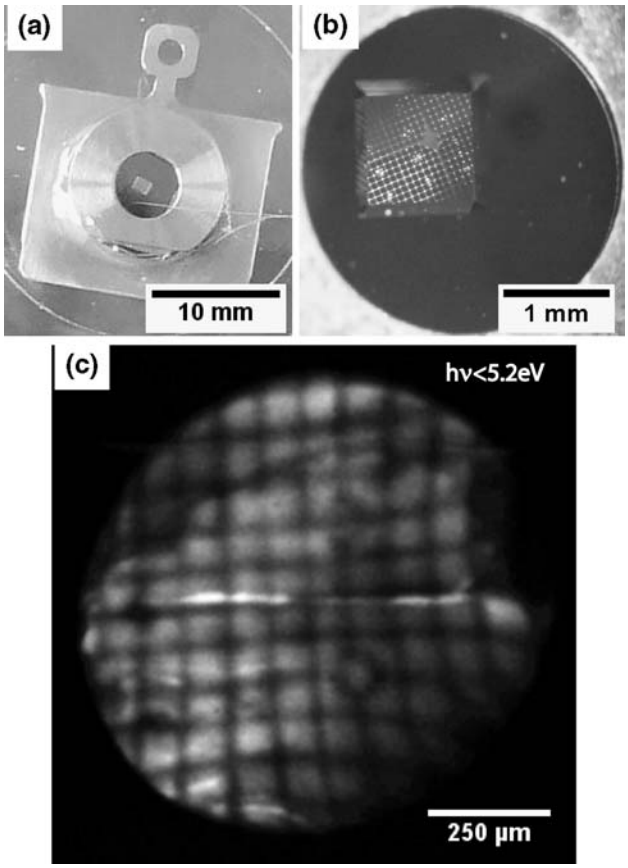

Fig. 3 **a** PEEM sample holder with implemented liquid cell; **b** enlarged view of the silicon nitride membrane with TEM grid behind; **c** laboratory T-PEEM image of a liquid protein sample; a mercury high-pressure UV lamp was used for illumination

Sample and sample preparation

While arthropod hemocyanins are built up by integer numbers of hexamers (2 × 6, 4 × 6, 6 × 6 and 8 × 6) depending on the species (Markl and Decker 1992), mollusc hemocyanin consists of ten subunits. Each subunit consists of seven to eight so-called "functional units". Depending on the species, decamers or dimerized didecamers are found. Each functional unit carries one active site (Van Holde and Miller 1995). Here, one molecule is reversibly bound as peroxide between two copper atoms in a side on coordination (Magnus et al. 1994; Cuff et al. 1998).

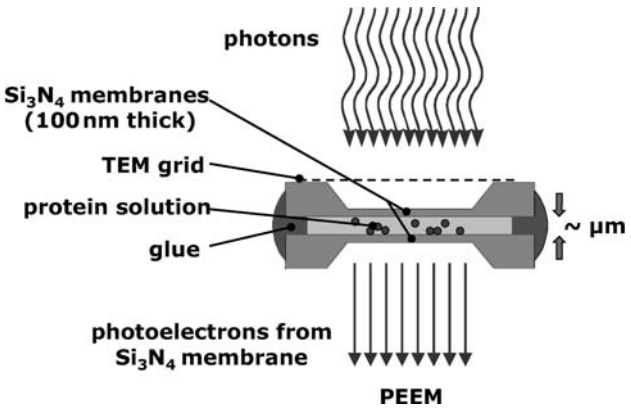

Fig. 2 Liquid sample cell construction for T-PEEM. The liquid protein sample is enclosed by two silicon nitride membranes on Si carriers. A TEM grid is mounted at the photon beam side to define a coordinate system in the PEEM image

We used the didecameric hemocyanin KLH1 of the giant keyhole limpet *megathura crenulata*. One hundred and sixty oxygen binding sites with their 320 copper atoms were distributed throughout the cylindric hemocyanin KLH1. Thus, about three to four copper atoms per $Å^2$ are transilluminated per KLH1. Upon oxygenation, large differences between the two conformations of KLH1 are observed (Hartmann and Decker 2004; Hartmann et al. 2004). In addition, the valence of the copper atoms changes upon oxygenation from Cu(I) to Cu(II) (the latter shown in Fig. 4), which is also accompanied by a switch in color from a transparent to a blue solution.

The liquid sample was prepared by transferring a droplet of KLH1 protein solution on top of a clean silicon nitride membrane. This membrane was subsequently enclosed by a

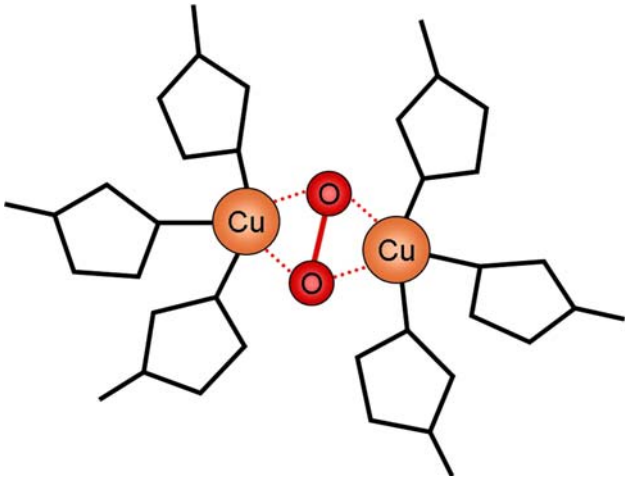

Fig. 4 Sketch of the copper active-site geometry for the oxygenated hemocyanin

second one as described in "The liquid sample cell". In our protein solution, a final KLH1 concentration of 20 mg/ml KLH1 hemocyanin was used.

Lateral X-Ray absorption structure mapping of copper in hemocyanin

Different approaches to the X-ray absorption spectroscopy (XAS, i.e., XANES spectroscocopy) of metalloproteins were chosen in the last years: for example, Sabatucci et al. (2002) performed hard X-ray XANES spectroscopy of hemocyanin powder samples in the X-ray range near the copper K-edge (~7 keV), whereas, for example, Freiwald et al. (2004) performed fluorescence yield soft X-ray XANES spectroscopy of metalloproteins.

In our approach, liquid sample handling under UHV conditions is combined with the PEEM imaging technique to gain lateral resolution. For soft X-ray absorption spectromicroscopy, linearly polarized undulator radiation from the monochromator beamline U41-PGM at BESSY II (Berlin) was used.

X-ray absorption spectroscopy near the L-edge of copper offers several advantages with respect to K-edge XAS: in comparison to the dipole-forbidden K-edge transitions (1 $s \rightarrow 3d$), L-edge transitions are dipole-allowed ($2p \rightarrow 3d$) and hence involve higher X-ray absorption cross sections. L-edge XAS is especially suited for studying ligand reactions in metalloproteins, such as hemeproteins, where the $3d$-orbitals are the ligand-bonding orbitals (Wang et al. 1997). These can be simulated by ligand field calculations, which provide detailed insight into the electronic structure of the metalloprotein (de Groot et al. 1990; de Groot 1994). In particular, L-edge XAS directly reflects the oxidation state and the spin state of the metal.

In Figure 5, a low magnification T-PEEM image of the KLH1 liquid cell is shown to be recorded at a photon energy of $h\nu = 930$ eV at the L_3 edge of copper. Here, the lateral resolution of ~10 µm poorly exploits the resolving capacity of the PEEM. In a similar T-PEEM setup, the lateral resolution was determined to ~65 nm (Pohl et al. 2004) but without exploiting chemical sensitivity. A total transillumination time of 30 s per image (1200 s per scan) was chosen because the delayline detector used is limited in count rate. This problem could be circumvented by using a more recent DLD version or by using the standard combination of MCP, fluorescence screen and CCD camera as imaging unit.

The grid pattern from a nickel TEM mask (Agar Scientific, G2730 N, grid spacing ~64 µm) is clearly visible, indicating a field of view of ~700 µm in diameter. The bright spot indicated by the label "C" originates from the residual X-ray beam, which traversed the liquid cell and the whole microscope column slightly off the electron optical axis. Note that the size of this photon signal refers to the plane of the imaging unit at the end of the microscope column and not to the position of the liquid cell. In contrast to the electron beam, this residual X-ray beam is not magnified by the PEEM.

For spectromicroscopy, a complete image set was recorded in the range from $h\nu = 920$ eV to $h\nu = 960$ eV with energy steps of $\Delta E = 1$ eV. This large energetic spacing is not related to the U41-PGM beamline monochromator

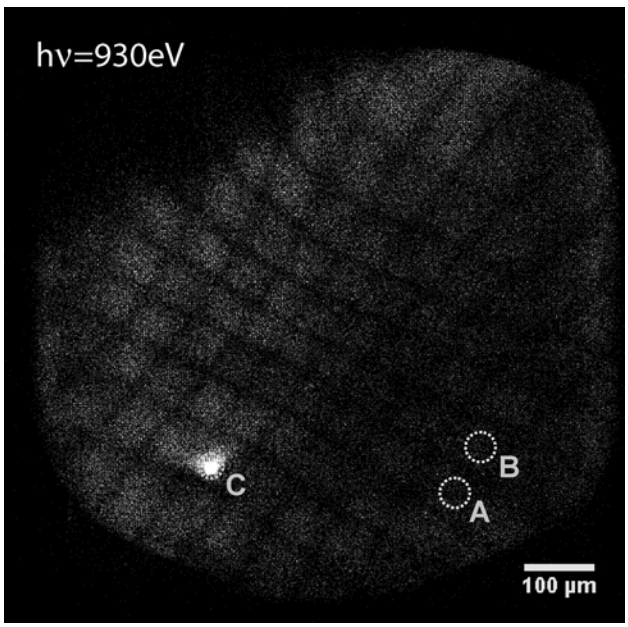

Fig. 5 T-PEEM image of the KLH liquid cell sample recorded at a photon energy of $h\nu = 930$ eV at the L_3 edge of copper. Microareas *A*, *B* are used for extraction of X-ray absorption signatures in the photoemission; microarea *C* displays the residual X-ray beam traversing the liquid cell and impinging on the detector. The *scale bar* refers to the center part of the PEEM image

energy resolution (E/ΔE ~ 2000), but was chosen here as a compromise between spectral information and radiation damage to the sample due to extended scanning times.

The photoelectron yield from restricted areas (encircled regions "A" and "B", ~40 μm in diameter) was then extracted from the complete image stack and plotted against the photon energy. Figure 6a shows the corresponding microarea XAS spectra in the photoemission. Two different copper species can be distinguished: spectrum "A" displays weak but significant absorption peaks predominantly at $h\nu = 930$ eV (L_3) and $h\nu = 949$ eV (L_2), which we attribute to Cu in the oxidation state +II (oxy state) (Grioni et al. 1989). Spectrum "B" exhibits two distinct absorption peaks, predominantly around $h\nu = 933$ eV (L_3) and $h\nu = 953$ eV (L_2), which we relate to copper in the oxidation states +I (deoxy state) (Grioni et al. 1989).In the case of Hc, this includes the presence of peroxidic oxygen bound in a side on coordination.

It is interesting to note that a copper XAS spectrum is also obtained from the microarea "C", that is, from the direct X-ray beam attenuation, which shows a superposition

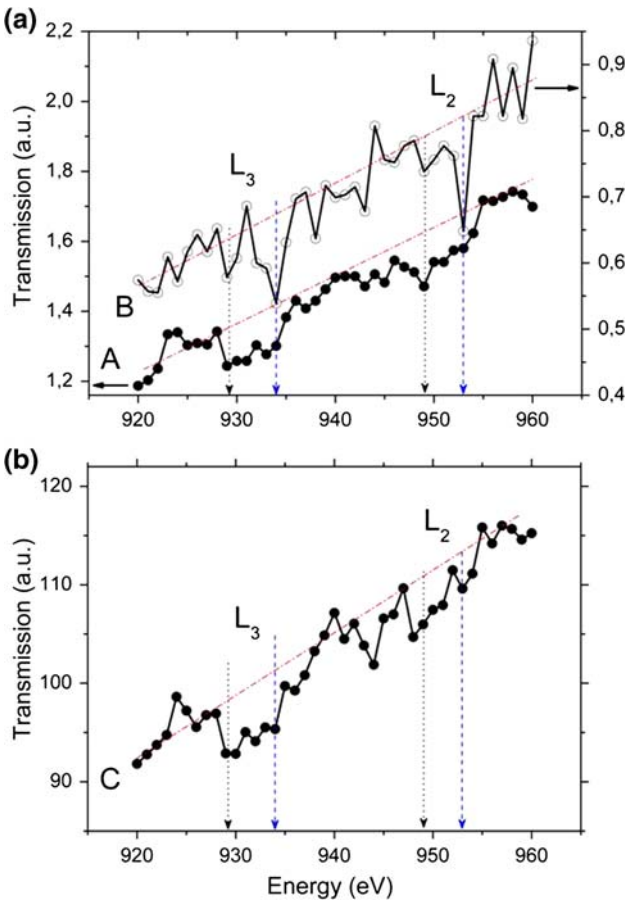

Fig. 6 Transmission spectra related to the X-ray absorption near the copper L-edge. **a** Spectral scans extracted from microareas *A*, *B* marked in Fig. 5. **b** Spectral scan extracted from the residual X-ray beam (microarea *C* in Fig. 5)

of Cu(I) and Cu(II), see Fig. 6b. As mentioned, this is not a local spectrum because it corresponds to the full photon beam.

The increase of denaturated protein during X-ray exposure is inevitable during XANES measurements and therefore needs to be treated with care. In order to minimize protein damages, several approaches were suggested: Ascone et al. (2000) embedded proteins in a saccharose-based matrix and demonstrated preservation of biological functionality of the protein after X-ray exposure, however in the hard X-ray regime. Denbeaux et al. (2001), for example, propose the usage of cryogenic protein samples to preserve their structural integrity. Finally, Sabatucci et al. (2002) chose a combination of both by first dissolving the protein in a sucrose-based matrix and then freezing the solution to obtain a cryogenic powder. It is worthwhile being mentioned that the Cu $L_{2/3}$ edges are not within "water window" usually used for X-ray microscopy of aqueous samples, that is the energy interval between the carbon K-edge ($h\nu \sim 284$ eV) and the oxygen K-edge ($h\nu \sim 543$ eV), where water absorbs approximately an order of magnitude less strongly than organic matter (Meyer-Ilse et al. 2001). However, a thin aqueous film with an estimated thickness of a few microns is obviously sufficiently transparent around $h\nu = 930$ eV.

At the present stage, the degree of radiation damage was not specified. However, it should be noted that the exposure time of 30 s per image appears rather long for the analysis of a biological sample. To minimize protein denaturation from X-ray exposure in the liquid cell, the proteins might be studied in a modified flow cell. This can initially be done without lateral resolution, for example, within the Liquidrom experiment at BESSY II by recording the total X-ray fluorescence yield from a flowing liquid at different photon energies. By this, reference data recorded under low X-ray exposure are accessible and would allow to characterize the binding states and the degree of X-ray damage more accurately for future laterally resolved analysis using T-PEEM.

Conclusions and outlook

We have presented first laterally resolved XAS measurements of a metalloprotein in solution using T-PEEM. Copper XAS structures are identified in various areas of interest. Different copper oxidation states are distinguished, suggesting sensitivity to the copper bonding within the protein. Clearly both lateral and energy resolution were not fully exploited in this initial work.

The T-PEEM may provide a method for studying metals in proteins "at work". In the case of hemocyanins, the change in the copper state switches from Cu(I) to Cu(II) upon oxygenation requires a different configuration at the

active site for coordinating the copper atoms and forcing the protein into a different conformation. Provided sufficient elemental sensitivity, small protein clusters (~100 nm) might be imaged with chemical sensitivity by T-PEEM in future work.

Further advances of the T-PEEM method for the laterally resolved chemical analysis of (metallo-) proteins might be achieved using functionalized membranes for binding the molecules to the surface and a flow-cell setup in order to minimize radiation damages.

Acknowledgments We gratefully acknowledge excellent beamtime assistance from C. Jung, BESSY GmbH and valuable support from A. Oelsner, Surface Concept GmbH. Further, we like to thank U. Kleineberg, Ludwig Maximilian-Universität München, for several silicon membranes that we used for laboratory tests in the early stage of our experiment, and J. Markl, Johannes Gutenberg-Universität Mainz, for the KLH hemocyanin. This project was funded by the Deutsche Forschungsgemeinschaft (DE 414/12-1 and SCHO 341/7).

References

Ade H (1998) X ray spectromicroscopy in vacuum ultraviolet spectroscopy. In: Samson JAR, Lederer DL (eds) Experimental methods in physical sciences, vol 32. Academic Press, London, pp 225

Ascone I, Sabatucci A, Bubacco I, Di Muro P, Salvato B (2000) Saccharose solid matrix embedded proteins: a new method for sample preparation for X-ray absorption spectroscopy. Eur Biophys J 29:391–397. doi:10.1007/s002490000088

Bauer E (2001) Photoelectron microscopy. J Phys Condens Matter 13:11391–12404. doi:10.1088/0953-8984/13/49/316

Chao W, Harteneck BD, Liddle JA, Andersson EH (2005) Soft X-ray microscopy at spatial resolution better than 15 nm. Nature 435:1210–1213. doi:10.1038/nature03719

Cuff ME, Miller KI, van Holde KE, Hendrickson WA (1998) Crystal structure of a functional unit from Octopus hemocyanin. J Mol Biol 278:855–870. doi:10.1006/jmbi.1998.1647

Decker H (2005) Copper proteins with dinuclear active sites. In: King BR (ed) The encyclopedia of inorganic chemistry, vol 2, 2nd edn. Wiley & sons, London, pp 1159–1173

de Groot FMF (1994) X-ray absorption and dichroism of transition metals and their compounds. J Electron Spectrosc Relat Phenom 67:529–622. doi:10.1016/0368-2048(93)02041-J

de Groot FMF, Fuggle JC, Thole BT, Sawatzky A (1990) 2*p* X-ray absorption of 3*d* transition-metal compounds: an atomic multiplet description including the crystal field. Phys Rev B 42:5459–5469. doi:10.1103/PhysRevB.42.5459

Denbeaux C et al (2001) Soft X-ray microscopy to 25 nm with applications to biology and magnetic materials. Nucl Instrum Methods Phys Res A 841:467–468

Freiwald M, Cramm S, Eberhard W, Eisebitt S (2004) Soft X-ray absorption spectroscopy in liquid environments. J Electron Spectrosc Relat Phenom 137–140:413–416. doi:10.1016/j.elspec.2004.02.165

Grioni M et al (1989) Study of copper valence states with Cu L_3 X-ray absorption spectroscopy. Phys Rev B 39:1541–1545. doi:10.1103/PhysRevB.39.1541

Hartmann H, Decker H (2004) Small angle scattering techniques for analyzing structural transitions in hemocyanins. In: Holt JM, Johnson ML, Ackers GK (eds) Methods in enzymology, vol 379. Academic Press, San Diego, pp 81–106

Hartmann H, Bongers A, Decker H (2004) Monte Carlo based reconstruction of keyhole limpet hemocyanin type I (KLH1): small angle X-ray scattering reveals oxygen dependent conformational changes of the surface. J Biol Chem 279:2841–2845. doi:10.1074/jbc.M308959200

Hitchcock AP, Morin C, Zhang X, Araki T, Dynes J, Stöver H et al (2005) Soft X-ray spectromicroscopy of biological and synthetic polymer systems. J Electron Spectrosc Relat Phenom 259:144–147

Magnus KA, Hazes B, Ton-That H, Bonaventura C, Bonaventura J, Hol WGJ (1994) Crystallographic analysis of oxygenated and deoxygenated states of arthropod hemocyanin shows unusual differences. Proteins 19:302–309. doi:10.1002/prot.340190405

Markl J, Decker H (1992) Molecular structure of the arthropod hemocyanins. Adv Comp Environ Physiol 13:325–376

Meyer-Ilse W et al (2001) High resolution protein localization using soft X-ray microscopy. J Microsc 201:395–403. doi:10.1046/j.1365-2818.2001.00845.x

Oelsner A et al (2001) Microspectroscopy and imaging using a delay line detector in time-of-flight photoemission microscopy. Rev Sci Instrum 72:3968–3974. doi:10.1063/1.1405781

Oelsner A, Krasyuk A, Fecher GH, Schneider CM, Schönhense G (2004) Image enhancement in photoemission electron microscopy by means of imaging time-of-flight analysis. J Electron Spectrosc Relat Phenom 137–140:757–761. doi:10.1016/j.elspec.2004.02.163

Pohl M, Kleineberg U, Heinzmann U (2004) Transmission photoelectron microscopy of diatoms at the multilayer monochromator beamline U125-1/ML at BESSY II. In: Warwick T et al (ed) Synchrotron Radiat Instrum 8th Int Conf, San Francisco, pp 1360–1363

Sabatucci A, Ascone I, Bubacco L, Beltramini M, Di Muro P, Salvato B (2002) Comparison of the X-ray absorption properties of the binuclear active site of molluscan and arthropodan hemocyanins. J Biol Inorg Chem 7:120–128. doi:10.1007/s007750100272

Schmidt T et al (2002) XPEEM with energy-filtering: advantages and first results from the SMART Project. Surf Rev Lett 9:223–232. doi:10.1142/S0218625X02001811

Schneider CM, Schönhense G (2002) Investigating surface magnetism by means of photoexcitation electron emission microscopy. Rep Prog Phys 65:R1785–R1839. doi:10.1088/0034-4885/65/12/202

Seah MP, Dench WA (1979) Quantitative electron spectroscopy of surfaces: a standard data base for electron inelastic mean free path in solids. Surf Interface Anal 1:2–11. doi:10.1002/sia.740010103

Solomon EI, Baldwin MJ, Lowery MD (1992) Electronic structures of active sites in copper proteins- contributions to reactivity. Chem Rev 92:521–542. doi:10.1021/cr00012a003

Stöhr J (1992) NEXAFS Spectroscopy, Springer, Berlin

Takeuchi A, Aoki S, Yamamoto K, Takano H, Watanabe N, Ando M (2000) Full-field x-ray fluorescence imaging microscope with a Wolter mirror. Rev Sci Instrum 71:1279–1285. doi:10.1063/1.1150454

Van Holde KE, Miller KI (1995) Hemocyanins. Adv Protein Chem 47:1–81

van Holde KE, Miller KI, Decker H (2001) Hemocyanins and invertebrate evolution. J Biol Chem 276:15563–15566. doi:10.1074/jbc.R100010200

Watts RN, Liang S, Levine ZH, Lucatorto TB, Polack F, Scheinfein MR (1997) A transmission x-ray microscope based on secondary-electron imaging. Rev Sci Instrum 68:3464–3476. doi:10.1063/1.1148309

Wang H et al (1997) Iron L-edge X-ray absorption spectroscopy of myoglobin complexes and photolysis products. J Am Chem Soc 119:4921–4928. doi:10.1021/ja961446b